ORIGINAL ARTICLE

# Direct Relay Pathways from Lemniscal Auditory Thalamus to Secondary Auditory Field in Mice

Shinpei Ohga[1], Hiroaki Tsukano ⑮ [1], Masao Horie[2], Hiroki Terashima[3], Nana Nishio[1], Yamato Kubota[4], Kuniyuki Takahashi[4], Ryuichi Hishida[1], Hirohide Takebayashi[5] and Katsuei Shibuki[1]

[1]Department of Neurophysiology, Brain Research Institute, Niigata University, 1-757 Asahimachi-dori, Chuo-ku, Niigata 951-8585, Japan, [2]Department of Morphological Sciences, Graduate School of Medical and Dental Sciences, Kagoshima University, 8-35-1 Sakuragaoka, Kagoshima 890-8544, Japan, [3]NTT Communication Science Laboratories, NTT Corporation, 3-1 Morinosato Wakamiya, Atsugi-shi, Kanagawa 243-0198, Japan, [4]Department of Otolaryngology, Graduate School of Medicine and Dental Sciences, Niigata University, 1-757 Asahimachi-dori, Chuo-ku, Niigata 951-8510, Japan and [5]Division of Neurobiology and Anatomy, Graduate School of Medicine and Dental Sciences, Niigata University, 1-757 Asahimachi-dori, Chuo-ku, Niigata 951-8510, Japan

Address correspondence to Hiroaki Tsukano, Department of Neurophysiology, Brain Research Institute, Niigata University, 1-757 Asahimachi-dori, Chuo-ku, Niigata 951-8585, Japan. E-mail: tsukano-nii@umin.ac.jp ⑮ orcid.org/0000-0001-8511-7256

## Abstract

Tonotopy is an essential functional organization in the mammalian auditory cortex, and its source in the primary auditory cortex (A1) is the incoming frequency-related topographical projections from the ventral division of the medial geniculate body (MGv). However, circuits that relay this functional organization to higher-order regions such as the secondary auditory field (A2) have yet to be identified. Here, we discovered a new pathway that projects directly from MGv to A2 in mice. Tonotopy was established in A2 even when primary fields including A1 were removed, which indicates that tonotopy in A2 can be established solely by thalamic input. Moreover, the structural nature of differing thalamocortical connections was consistent with the functional organization of the target regions in the auditory cortex. Retrograde tracing revealed that the region of MGv input to a local area in A2 was broader than the region of MGv input to A1. Consistent with this anatomy, two-photon calcium imaging revealed that neuronal responses in the thalamocortical recipient layer of A2 showed wider bandwidth and greater heterogeneity of the best frequency distribution than those of A1. The current study demonstrates a new thalamocortical pathway that relays frequency information to A2 on the basis of the MGv compartmentalization.

Key words: compartmentalization, mice, secondary auditory field, tonotopy, ventral division of the medial geniculate body

## Introduction

The auditory cortex is composed of multiple regions that form a hierarchy of information processing; tonal information enters at primary cortex and is then relayed to higher-order cortex in streams of increasing complexity (Kaas and Hackett 2000). Primary auditory cortex exhibits tonotopy that reflects

information directly relayed from topographically connected lemniscal pathways that ascend from the periphery through the ventral division (MGv) of the medial geniculate body (MGB) (Saenz and Langers 2014). In contrast, higher-order regions may not show tonotopy because they receive much of their input from the higher-order, non-lemniscal dorsal division (MGd) of MGB, which is not tonotopic. This exclusive, parallel pathway model, in which one pathway connects MGv to primary regions and the other connects MGd to higher-order regions, has been a basic tenet of auditory system research for the last two decades in several animal species, including monkeys (de la Mothe et al. 2012), cats (Huang and Winer 2000), rats (Smith et al. 2012), and mice (Llano and Sherman 2008).

The primary auditory cortex (A1) and secondary auditory field (A2) are regarded as representatives of primary and higher-order auditory regions, respectively, and exemplify the auditory cortex hierarchy across species (Lee and Sherman 2008, 2010; Lee and Winer 2008a, 2008b; Issa et al., 2014). For mice in particular, A1 and A2 are thought to exhibit a cortical hierarchy that is reflected in different response latencies (Guo et al. 2012; Joachimsthaler et al. 2014) and in different levels of tonotopic complexity in their respective layers 2/3 (Issa et al. 2014). Recently, higher-order regions beyond A1 have been shown to reflect tonotopy in different mammalian species, and thus multiple tonotopic representations are now thought to exist within the auditory cortex (Harel et al. 2000; Kalatsky et al. 2005; Petkov et al. 2006; Nishimura et al. 2007; Bizley and King 2009; Higgins et al. 2010). Mouse A2 also exhibits tonotopy (Kubota et al. 2008; Issa et al. 2014; Kato et al. 2015), which is presumed to incorporate information relayed from lemniscal regions. However, these theorized topographical projections that determine tonotopy in mouse A2 have yet to be identified.

Recent developments in auditory thalamocortical research suggest the possibility that tonotopy in A2 might inherit that in the lemniscal thalamus. In canonical theories, A1 and A2 have an intracortical hierarchical relationship in which tonotopy in A2 is derived from secondary connections originating in A1. Thus, mouse A2 should receive frequency-related projections from A1 that are topographically-arranged, similar to how mouse primary visual cortex topographically projects to secondary visual cortices (Wang and Burkhalter 2007; Glickfeld et al. 2013). Another possibility is that tonotopy in A2 is based on input from MGv that reflects its subcortical functional organization, as has been demonstrated between MGv and A1 (Hackett et al. 2011). Recent tracing studies suggest that the lemniscal thalamocortical pathway is actually composed of several different parallel pathways. Rather than being a single homogenous structure, MGv is composed of multiple compartments, each of which sends frequency-related topographical projections to distinct cortical targets (Horie et al. 2013; Takemoto et al. 2014; Tsukano et al. 2015). At present, the thalamic origins of four cortical tonotopic regions (not including A2) have been identified in rostral and middle parts of MGv (Takemoto et al. 2014; Tsukano et al. 2015). Considering that A2 is the last tonotopic field whose thalamic origin has not yet been deeply investigated in mice and that the cortical target of neurons located in the caudal portion of MGv remains unknown, we hypothesized that A2 receives topographically-arranged auditory input from the caudal compartment of MGv. To test this hypothesis, we used a combination of retrograde tracing and precise identification of A2 using flavoprotein fluorescence optical imaging.

Differences in regional properties between A1 and A2 can be seen in tonotopic organization at the single neuron level, in which neighboring neurons are heterogeneously tuned to dissimilar best frequencies (BFs) (Bandyopadhyay et al. 2010; Castro and Kandler 2010; Rothschild et al. 2010; Tao et al. 2017). Specifically, the extent of heterogeneous tuning within layer 2/3 follows a hierarchy, becoming larger in A2 than in A1 (Issa et al. 2014). Although the origin of this region-specific functional organization is unclear, it is likely formed by a mechanism that depends on exogenous input and intrinsic local circuits. The intrinsic cortical mechanism for tuning neurons has already been found in cortical layer 2/3 (Kato et al. 2017). We hypothesized that the heterogeneity of neighboring BFs in thalamo-recipient layers is also derived from exogenous input patterns that originate in MGv. If this is true, then functional organization in the thalamo-recipient layer should reflect the anatomical patterns of the thalamocortical projections (Storace et al. 2011; Imaizumi and Lee 2014), thus potentially explaining the locally heterogeneous frequency inputs (Vasquez-Lopez et al. 2017).

In the current study, we show that the major thalamic origin of mouse A2 is the caudal part of MGv (Fig. 9). A2 and caudal MGv are topographically connected, and tonotopy in A2 can be established via thalamic inputs in the absence of corticocortical inputs from A1. We also show that local areas in A2 receive thalamocortical inputs from a larger region of MGv than does A1, and that the tonotopy of the thalamocortical recipient layer 3b/4 is correspondingly more heterogeneous in A2 than in A1.

## Materials and Methods

### Animals

This study was conducted in accordance with the approved protocols and guidelines of the Committee for Animal Care in Niigata University. We used 6–7-week old male C57BL/6 N mice (Charles River Japan, Kanagawa, Japan). Mice were housed in cages under a 12 h light/dark cycle with *ad libitum* access to food pellets and water.

### Flavoprotein Fluorescence Imaging

Flavoprotein fluorescence imaging was performed according to methods described in our previous studies (Horie et al. 2013; Tsukano et al. 2015). Mice were anesthetized with urethane (1.65 g/kg, i.p.) and rectal temperature was kept at ~37.0 °C. After subcutaneous injection of bupivacaine, the skin and temporal muscle were removed. A piece of metal was attached to the skull with dental resin, and the head was fixed by screwing the metal piece onto a manipulator. Unless otherwise noticed, a ~3 × 3-mm craniotomy was performed over the right auditory cortex. Because C57BL/6 mice have no significant laterality differences in the size of the auditory cortex (Tsukano et al. 2016), and because auditory cortical subregions that correspond interhemispherically are located along symmetrical stereotaxic coordinates (Horie et al. 2015), either hemisphere is available for revealing macroscopic- and mesoscopic-scale neuroanatomical structures: therefore, the current study chose to investigate the thalamocortical circuitry in the right hemisphere to be consistent with successive neuroanatomical studies in the mouse thalamocortical pathway (Horie et al. 2013; Tsukano et al. 2015; Tsukano et al. 2017b). For transcranial imaging (Fig. 1), the skull over the right auditory cortex was intact and kept transparent using liquid paraffin. Cortical images (128 × 168 pixels after binning) of endogenous green fluorescence ($\lambda$ = 500–550 nm) in blue light ($\lambda$ = 470–490 nm) were recorded at 9 Hz using a cooled charge-coupled device (CCD) camera system (AQUACOSMOS with ORCA-R2 camera;
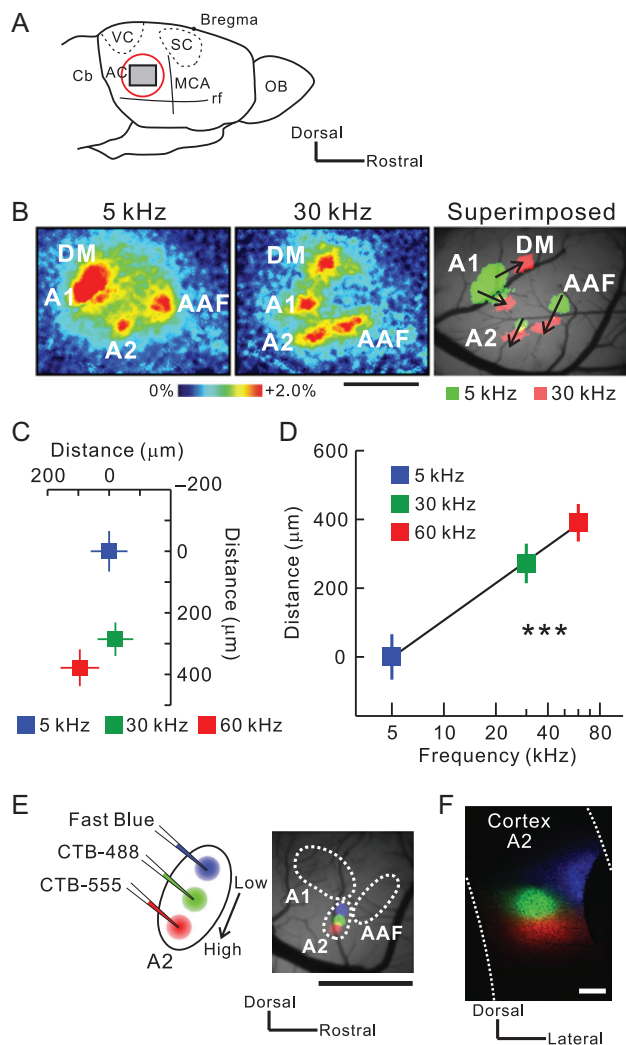
**Figure 1.** Injection of retrograde tracers along the tonotopic map in mouse A2. (A) A schematic drawing of the mouse auditory cortex. AC, auditory cortex; Cb, cerebellum; MCA, medial cerebral artery; OB, olfactory bulb; rf, rhinal fissure; SC, somatosensory cortex; VC, visual cortex. (B) Typical images of tonal responses in the auditory cortex revealed using flavoprotein fluorescence imaging. Scale bar, 1 mm. (C) The tonotopic organization of A2. The averaged location of pixels with peak fluorescence is plotted in response to different frequencies. Significant shifts in response were observed from dorsal to ventral A2. Data were obtained from nine mice and superimposed based on the pixel of an A1 5-kHz response peak. (D) Correlation between frequencies and distances. Tonotopy was arranged along the axis connecting the peak pixels for 5-kHz and 60-kHz tones. $r = 0.66$, ***$P < 0.001$, Spearman's test; $n = 9$ each. (E) Triple injection of Fast Blue (blue), CTB-488 (green), and CTB-555 (red) along the tonotopic gradient of A2. Tracer deposits on the brain surface ~30 min after injection are shown on the right. Scale bar, 1 mm. (F) Tracer deposits in A2 on a coronal slice. Scale bar, 200 μm. Data are shown in mean ± SEM.

Hamamatsu Photonics, Shizuoka, Japan) that was attached to an epifluorescence microscope (M651; Leica, Wetzlar, Germany). Images were averaged over 20 trials. Fluorescence responses were normalized as $\Delta F/F_0$, where $F_0$ represents the average of five images (~500 ms) before stimulus onset.

## Neuronal Tracer Injections

We used Fast Blue (Funakoshi, Tokyo, Japan), Alexa Fluor-488, and Alexa Fluor-555 conjugated cholera toxin B subunits (CTB) (Invitrogen, Thermo Fisher Scientific, Boston, MA) as a

retrograde neural tracer. We performed triple injections of Fast Blue, CTB-488, and CTB-555, or dual injections of CTB-488 and CTB-555, or a single injection of CTB-555. Before injection, precise locations of auditory regions were identified using flavoprotein fluorescence imaging. A glass pipette (tip: 20–30 μm) filled with a tracer was inserted ~400 μm down into an identified area. One of the tracers was then injected iontophoretically with a 5-μA anodal current (5 s on, 5 s off) having ~100 pulses. After the injection, the glass pipette was slowly withdrawn and the skin was sutured. Mice were placed in a warm place for recovery, and after awaking they were reared in their home cages.

## Tracer Observation

Three days after injection, mice were anesthetized with an overdose of pentobarbital (0.3 g/kg), and cardiac perfusion was performed using 4% paraformaldehyde. After sequential immersion into 20% and 30% sucrose solutions, coronal, or horizontal brain slices were prepared at 40-μm intervals according to our previous studies (Horie et al. 2013, 2015). Every fourth slice was mounted on a glass slide and cover-slipped using Fluoromount (Cosmo Bio, Tokyo, Japan). Sections were observed using a light microscope (Eclipse Ni, Nikon, Tokyo, Japan) and a CCD camera (DP-80; Olympus, Tokyo, Japan). After observing fluorescent tracers, sections were Nissl-stained as described in Horie et al. (2013), and cover-slipped using Bioleit (Okenshoji, Tokyo, Japan).

## Suction Injury

After identifying the locations of auditory regions using optical imaging, we lesioned the auditory cortex by slowly sucking away all layers using a glass pipette (tip diameter: ~70 μm) connected to a vacuum pump. Suction was stopped at the depth where the parenchyma turned whitish in color, which indicated the white matter beneath the auditory cortex had been reached. After completing the suction, the hole was covered with 2% agarose (1-B, Sigma-Aldrich, MO) and a thin cover glass (thickness <0.15 mm, Matsunami, Osaka, Japan), which was fixed to the skull with dental cement (Sun Medical, Shiga, Japan). The tonal responses of A2 were recorded about three hours after completing the suction injury.

## Partition of the MGB Subdivisions

The borders of the medial geniculate body (MGB) subdivisions were drawn according to the mouse brain atlas (Paxinos and Franklin 2012) and SMI-32 immunolabeling patterns, which recognize a non-phosphorylated epitope on the 168- and 200-kDa subunits of neurofilament proteins (LeDoux et al. 1985, 1987; Honma et al. 2013; Horie et al. 2013, 2015). SMI-32 immunolabeling was performed in adjacent sections. Sections were rinsed and incubated in phosphate-buffered saline with Triton X-100 (PBST) containing 3% hydrogen peroxide. After rinsing in 20 mM PBS, the sections were incubated overnight at room temperature with the mouse monoclonal antibody SMI-32 (1:2 000, Covance Research Products, Berkeley, CA) and diluted with 20 mM PBS containing 0.5% skim milk. Sections were then incubated with horseradish peroxidase (HRP)-labeled anti-mouse IgG (1:100, MBL, Nagoya, Japan) at room temperature for 2 h, rinsed in 20 mM PBS, and then immunoreactions were visualized in a Tris-HCl buffer containing 0.05% diaminobenzidine tetrahydrochloride and 0.003% hydrogen peroxide for 4–5 min.

SMI-32-guided parceling was confirmed by conducting calbindin and calretinin immunolabeling. For calbindin immunolabeling, we used anti-calbindin primary antibody (1:10 000; ab11426, Abcam, Cambridge, UK) and HRP-labeled anti-Rabbit IgG as a secondary antibody (1:100; Invitrogen Life Technologies, Boston, MA). The remaining protocols were the same as those used to visualize SMI-32. For calretinin immunofluorescence labeling, we used anti-calretinin primary antibody (1:10 000; 6B3, Swant, Marly, Switzerland) and Alexa Fluor-488 conjugated anti-mouse IgG as a secondary antibody (1:100; ab150113).

## Separation Index

To quantify and compare the degree of spatial overlap between two neuronal populations, we used the absolute value of Cliff's delta (Cliff 1993) as a Separation Index (SI). Cliff's delta is a nonparametric metric of an effect size described in the following formula,

$$\delta = \frac{\#(x_1 > x_2) - \#(x_1 < x_2)}{n_1 n_2}$$

where $n_i$ is the size of group $i$ ($i = 1, 2$) and $\#(x_i > x_j)$ is an operator that counts the number of all possible combinations such that an item of Group 1 is greater than that of Group 2. It follows that Cliff's delta ranges from –1 to 1 and the three extreme conditions are

$$\delta = \begin{cases} +1 & if\ Group1_i > Group2_j,\ \forall_i,\ \forall_j \\ 0 & if\ Group1 = Group2 \\ -1 & if\ Group1_i < Group2_j,\ \forall_i,\ \forall_j \end{cases}$$

Because we did not need to discriminate the direction of difference in our analysis, we defined SI as the absolute value of Cliff's delta. This value ranges from 0 to 1, with 0 indicating that the locations of the two groups completely overlap and one indicating that they are completely separate without any overlap.

## In vivo Two-Photon Calcium Imaging

After inducing anesthesia with urethane (1.9 g/kg, i.p.) and performing a craniotomy of the right auditory cortex, the locations of A1 and A2 were identified using flavoprotein fluorescence imaging. Then, calcium imaging was performed using a two-photon microscope (TCS SP5 MP, Leica Microsystems, Wetzlar, Germany) with a hybrid detector (HyD, Leica Microsystems) and a Ti-Sapphire mode-locked femtosecond laser (Chameleon Vision, Coherent, Santa Clara, CA). Images were obtained via a × 20 water-immersion objective lens (numerical aperture 1.0, HCX PL APO; Leica Microsystems). We used Cal-520 as a calcium indicator for the following reasons. First, it exhibits a high signal-to-noise ratio and its event-related change in fluorescence is strongly correlated with spike number (Tada et al., 2014; Li et al., 2017). Second, Cal-520 is one of the fastest calcium indicators because of its short rise time (Lock et al. 2015). Third, frequency tuning and tonotopic organization in the auditory cortex are not greatly affected under anesthesia or in awake conditions when evaluated using Cal-520 (Li et al. 2017). Lastly, neuropil signals at the soma are not contaminated when using Cal-520 (Li et al. 2017). Cal-520 AM (Invitrogen, Thermo Fisher Scientific) was dissolved in 10% (w/v) Pluronic F-127 in DMSO and diluted with Ringer solution containing sulforhodamine 101 (SR-101, Invitrogen, Thermo Fisher Scientific).

Before injecting the Cal-520 solution, the cortical surface was observed via reflection mode using a 633-nm He-Ne laser that was built attached to the two-photon microscope. In this way, we could confirm the precise locations of A1 and A2 using the same vascular patterns that were identified using flavoprotein fluorescence imaging (Supplementary Fig. 8A). The Cal-520 solution was pressure-injected (5–20 kPa) for 5–10 min into A1 and A2 layer 3b/4 using glass pipettes (tip diameter: 2–4 μm). Astrocytes were distinguished from neurons using SR-101. After injection, the pipette was withdrawn and the craniotomy was covered with 2% agarose (1-B, Sigma-Aldrich) and a thin cover glass (thickness <0.15 mm, Matsunami), which was fixed to the skull with dental cement (Sunmedical). The excitation wavelength for Cal-520 was 900 nm and that for SR-101 was 940–950 nm. Cal-520 fluorescence was observed between 500 and 550 nm. Images (256 × 256 pixels) were recorded at 3.7 Hz in a 246 × 246-μm region. Rectal temperature of mice was kept at ~37.0 °C.

Data were analyzed using AQUACOSMOS and custom-written MATLAB code (Mathworks, St. Louise, MO). Data from 5 to 6 repeated trials of the same stimulation were averaged. The size of a region of interest (ROI) was set according to the size of the identified neurons. Data were calculated as $\Delta F/F_0$, where $\Delta F = F - F_0$, and $F_0$ (the baseline intensity) was obtained by averaging the intensity values during the pre-stimulus period (~3 s) across the repeated trials. The response of each neuron was evaluated in poststimulus observation windows (~5 s). Neurons were defined as responsive when the largest calcium response to presentations of 4–64 kHz tones was at least four standard deviations (SDs) above the baselines (Supplementary Fig. 8B). The BF of a neuron was defined as the frequency to which the neuron had the greatest response. The correlation between BF and location was calculated every 1 degree, and determined the direction of frequency organization as that which generated the largest correlation coefficient. Bandwidth of the tuning curves was defined as the logarithmic ratio between minimum and maximum frequencies that resulted in a response >75% of the peak amplitude. To merge neuronal distribution data across animals, we set the origin as the peak pixels of the 5-kHz area that was identified in A1 or A2 using prior flavoprotein fluorescence imaging.

## Auditory Stimuli

Tones were generated by a computer using a custom-written LabVIEW code (National Instruments, Austin, TX). The sampling rate was 500 kHz. Sounds were low-pass filtered at 150 kHz (3624, NF, Kanagawa, Japan). Pure tones at frequencies of 5–80 kHz were amplitude modulated by a 20-Hz sine wave. A speaker for 5–40-kHz (SRS-3050A, Stax, Saitama, Japan) or 50–80-kHz (ES105A, Murata, Kyoto, Japan) tones was set 10 cm in front of the mice. Sound intensity was calibrated using a microphone (Type 4135 and Type 2669, Brüel & Kjær, Nærum, Denmark) and a sound-level meter (Type 2610, Brüel & Kjær). The sound intensity was set to 60 dB SPL, and the duration was 500 ms with a rise/fall time of 10 ms. The desired sound spectrum was confirmed using a digital spectrum analyzer (R9211 A, Advantest, Tokyo, Japan) or a custom-written LabVIEW program.

## Statistics

Statistical analyses were conducted using MATLAB scripts, and SPSS (IBM Corp, Armonk, NY) if necessary. The Mann–Whitney U-test or the Wilcoxon signed-rank test was used to evaluate

differences between two paired or unpaired two groups, respectively. The $\chi^2$ test was used to evaluate differences in proportions of neurons. Correlations were evaluated using Spearman's test. The Kolmogorv–Smirnov test was used to evaluate the differences between two cumulative distributions. When multiple comparisons were needed, we used Bonferroni correction. We evaluated the differences between two correlation coefficients according to Howell (2012). Briefly, two $r$-values were $z$-transformed by the function $z = atanh(r)$ and the Z test statistic was calculated as

$$Z = \left| \frac{z_1 - z_2}{\sqrt{\frac{1}{n_1 - 3} + \frac{1}{n_2 - 3}}} \right|$$

$P$-values were obtained by the formula,

$$p = 2 \times (1 - F(Z)),$$

where $F(Z)$ is the normal cumulative distribution function of $Z$.

If MATLAB provided $P$-values of zero in any statistical analysis, we replaced them with $P < 10^{-35}$, because null hypotheses cannot be rejected with a probability of 100%.

## Results

### Mouse A2 Receives Inputs from Primary Thalamic Division, MGv

We identified the precise location of right auditory cortical regions using flavoprotein fluorescence imaging (Fig. 1A). Tonal stimuli around 5 kHz are known to produce neuronal responses in three regions. Numerous studies of mouse auditory cortex consider the dorsal two regions as the anterior auditory field (AAF) and A1, and the ventral region as A2 (Fig. 1B) (Stiebler et al. 1997; Guo et al. 2012; Issa et al. 2014; Joachimsthaler et al. 2014; Kato et al. 2015; Tsukano et al. 2015, 2016). In addition to these three areas, the dorsomedial field (DM) was also activated (Fig. 1B). Quantitative analysis of A2 using 5-kHz, 30-kHz, and 60-kHz tones indicated that the peak fluorescence change shifted from dorsal to ventral with increased tonal frequency (Fig. 1C,D), as previously reported (Kubota et al. 2008; Issa et al. 2014; Kato et al. 2015). To investigate the origin of thalamic input to A2, we injected retrograde tracers into A2 after regional identification using optical imaging. We triple injected Fast Blue, CTB-488, and CTB-555 (Takemoto et al. 2014) along the tonotopic axis of A2 (Fig. 1E,F), prepared consecutive coronal sections, and then visualized fluorescence-positive thalamic neurons. A low magnification image of an injection site is shown in Supplementary Fig. 1.

The boundary between MGv and MGd can be determined based on immunoreactivity (Lu et al. 2009). Here, we used SMI-32 immunolabeling that strongly stains MGv but not MGd (Fig. 2A) (Horie et al. 2013; Tsukano et al. 2015). In addition, SMI-32-based parceling was confirmed using calretinin and calbindin immunolabeling that strongly stains MGd and does not stain MGv (Fig. 2A and 3A; Lu et al. 2009; Takemoto et al. 2014). We found retrogradely-labeled neurons in MGd as shown in previous reports. Moreover, we observed numerous retrogradely-labeled neurons in MGv, especially in the caudal region (Fig. 2B). Here, we must be careful in what we mean by the caudal end of MGv. Although atlases illustrate MGv reaching the caudal end of MGB, the most caudal part of MGB is actually calretinin-positive (Allen Brain Atlas 2011), which indicates that MGv is actually shorter rostrocaudally than the atlases illustrate. In the current

study, we confirmed that calretinin immunoreactive signals in areas indicated as MGv were negative until about 3.6 mm posterior to the bregma; however, they became abruptly positive in the region caudal to this level (Fig. 3A,B). These data indicate that MGv can be localized to about 3.6 mm posterior to the bregma, while the more caudal part of MGB is a non-lemniscal division. Here, we refer to this non-lemniscal region as the caudal non-lemniscal pole of MGB.

Next, we dual visualized calretinin and CTB-555 injected into the middle frequency part of A2, and found that many CTB-555-positive neurons were located within MGv where calretinin signals were negative (Fig. 3C). These data directly confirm that neurons within MGv do project to A2. On the basis of the knowledge that MGv ends at ~3.6 mm posterior to the bregma, we counted retrogradely-labeled neurons in MGB using 43 coronal slices after injecting retrograde tracers into A2. Among the labeled neurons, 53.9% (3 901/7 238 neurons) were found in MGv, 18.7% (1 351/7 238 neurons) in MGd, 9.9% (713/7 238 neurons) in the caudal non-lemniscal pole, and 17.6% (1 273/7 238 neurons) in the rest of the auditory thalamus.

We next quantitatively analyzed the rostrocaudal distribution of projection neurons in MGv, which were primarily located between 3.3 and 3.6 mm posterior to the bregma (Fig. 4A). We found some labeled neurons in the caudal non-lemniscal pole as well. AAF and A1 are known to receive thalamic input from the middle part of MGv, around 2.9 to 3.2 mm posterior to the bregma (Horie et al. 2013; Takemoto et al. 2014; Tsukano et al. 2017a). We found that neurons projecting to A2 were clearly located caudal to those projecting to AAF/A1 (Fig. 4B). We directly confirmed the rostrocaudal locations of thalamic neurons by preparing horizontal slices (Fig. 4C). These results clearly indicated that mouse A2 receives lemniscal projections originating from the caudal part of MGv.

Next, we investigated whether neurons projecting to A2 are arranged in a frequency-related fashion. Using coronal slices, we obtained the relative location of each fluorescence-positive neuron in reference to the MGv center (Fig. 5A). MGv neurons projecting to the low, middle, and high frequency areas of A2 were topographically arranged in the ventrodorsal direction of caudal MGv (Fig. 5B). We found that overall positions shifted ventrally and medially in caudal slices (Fig. 5C); therefore, we evaluated frequency-related positional shifts using horizontal slices. We injected CTB-555 and CTB-488 into high and low frequency areas of A2. In the dorsal part of MGv, almost all neurons projected to high frequency areas (Fig. 5D). Moving ventrally, neurons projecting to low frequency areas began to appear rostral to those projecting to high frequency areas (Fig. 5E). Going more ventrally, neurons projecting to high and low frequency areas were evenly distributed (Fig. 5F). In the ventral part, we found that neurons projecting to high frequency areas were shoved caudally (Fig. 5G). These data suggest that the caudal compartment of MGv has a distinct frequency-related structure, and that the gradient is arranged largely along a ventrorostral to dorsocaudal axis, as shown in the parasagittal illustration in Figure 5H. This architecture is consistent with the findings obtained from the coronal slices, which showed that MGv neurons projecting to higher frequency areas of A2 tended to be located more caudally (Fig. 4A).

To determine whether any cortical areas receive thalamic inputs exclusively from MGd, we injected CTB-555 into the brain around the temporal association area (TeA)/ectorhinal cortex (ECT) ventral to the auditory cortex (Supplementary Fig. 2). We found that TeA/Ect received clear projections from the auditory thalamus, and almost all the CTB-555-positive
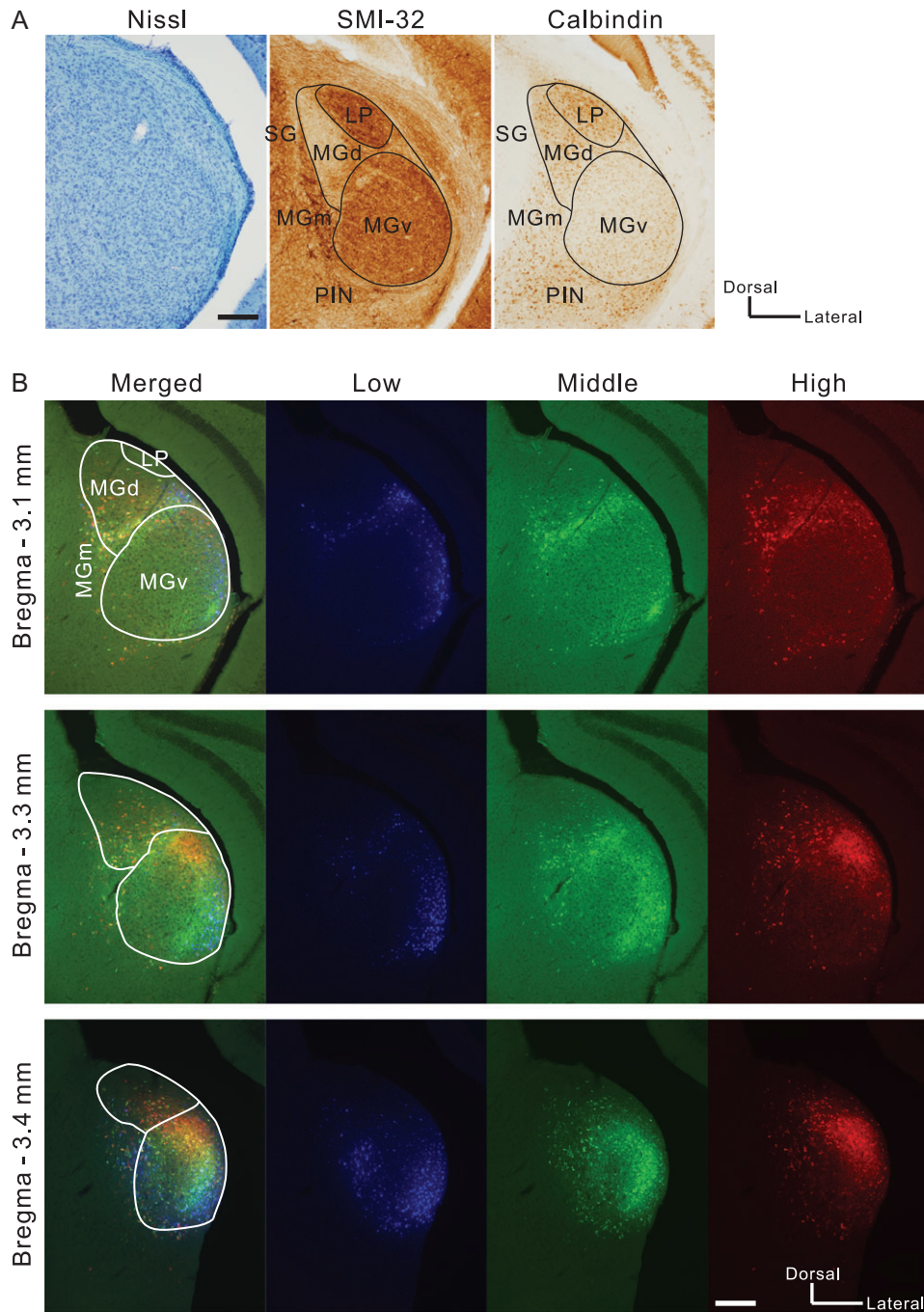
**Figure 2.** Visualizing thalamic neurons that project to A2. (A) An example pair of Nissl staining and immunolabeling in slices ~3.0 mm posterior to the bregma. These images were obtained from a single animal. LP, lateral posterior nucleus; PIN, posterior intralaminar nucleus; SG, suprageniculate nucleus. Scale bar, 200 μm. (B) Distribution of neurons that were labeled with tracers injected into A2. Blue, green, and red neurons gave rise to projections to low, middle, and high frequency areas, respectively in A2. Scale bar, 200 μm.

neurons were located within MGd. This finding is interesting because TeA/Ect is located outside the auditory cortex; however, it is consistent with Cai et al. (2018). Next, we injected CTB-555 into the ventrocaudal corner of the auditory cortex (Supplementary Fig. 3). This region is located ventral to a low frequency area of A1 and may correspond to an auditory region that has been termed the ventral-posterior field (VP) in Liu et al. (2017). Although we found only a few CTB-555-positive neurons within MGv, we found many more in comparatively caudal parts

of MGd, and in the caudal non-lemniscal pole of MGB. Here, we noticed that two MGd neuronal populations visualized by injecting CTB-555 into TeA/Ect and the cortex ventral to a low frequency area of A1 are located in mediolaterally different locations (Supplementary Figs. 2 and 3), which suggests that, like MGv, MGd may also be compartmentalized according to cortical target. Overall, these data imply the possibility that, besides A2, there exist additional higher-order auditory regions that have not yet been characterized.
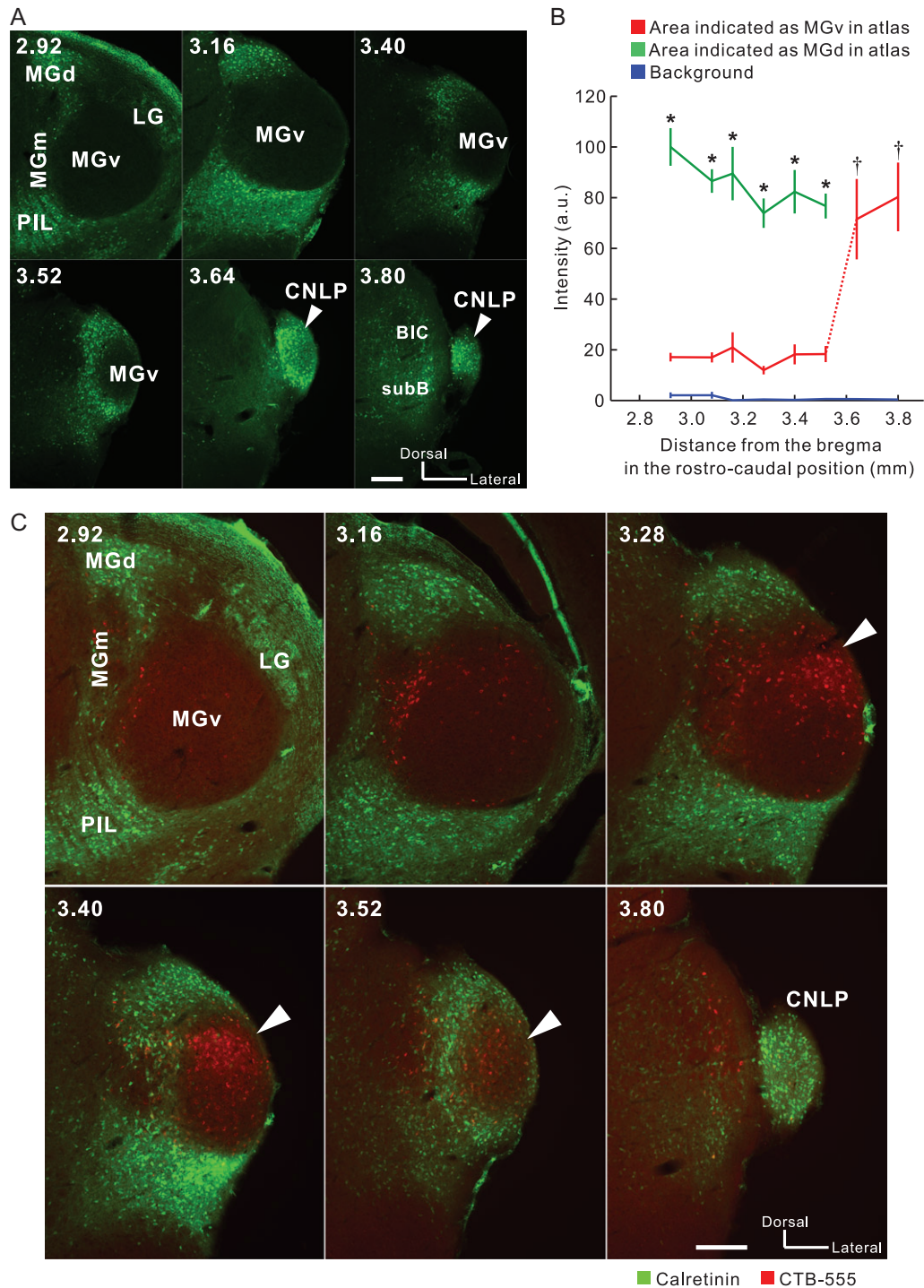
**Figure 3.** Presence of MGv neurons that directly project to A2. (A) Calretinin immunolabeling in coronal slices of MGB. MGv lacked calretinin signals while non-lemniscal divisions specifically exhibited strong calretinin signals. White arrow heads indicate calretinin-positive signals in the region that is typically illustrated as MGv in existing atlases. The numbers in the upper left indicate the distance from the bregma. BIC, brachium inferior colliculus; CNLP, caudal non-lemniscal pole; SubB, subbrachial nucleus Scale bar, 200 μm. (B) Quantitative analysis of fluorescence intensity in coronal MGv, MGd, and the caudal pole of MGB in the rostrocaudal direction. Values of intensity were obtained by putting ~150- × 150-μm ROIs on 8-bit images. At every level rostral to 3.6 mm posterior to the bregma, intensity values were larger in MGd than in MGv (*P < 0.05, Mann–Whitney U-test). Intensity values in the caudal pole of MGB were similar to those in MGd, and larger than those in MGv rostral to 3.6 mm posterior to the bregma (†P < 0.01, one-way ANOVA followed by Tukey–Kramer post hoc test). The data were obtained from four animals. (C) Dual visualization of calretinin and CTB-555 injected into the middle frequency area of A2. White arrowheads indicate CTB-positive neurons densely localized within MGv. LG, lateral geniculate body; PIL, posterior intralaminar thalamic nucleus. Scale bar, 200 μm.
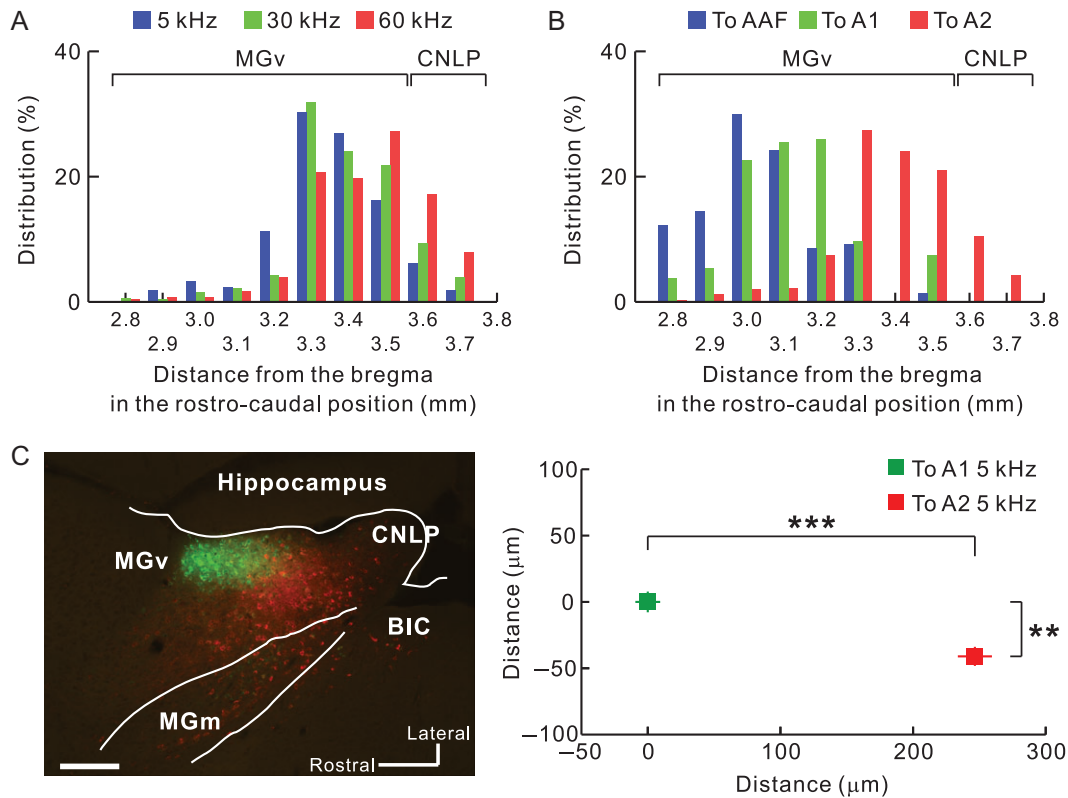
**Figure 4.** Quantification of the distribution of MGv neurons projecting to A2. (A) Rostrocaudal distribution of thalamic neurons projecting from MGv to A2. Averaged coordinates were 3.34 mm, 3.39 mm, and 3.43 mm posterior to the bregma for low, middle, and high frequencies, respectively. According to the analysis shown in Figure 3, labeled neurons caudal to 3.6 mm posterior to the bregma were classified as being part of the caudal non-lemniscal pole. 5 kHz vs. 30 kHz, $P < 10^{-6}$; 5 kHz vs. 60 kHz, $P < 10^{-35}$; 30 kHz vs. 60 kHz, $P < 10^{-5}$, $\chi^2$ test after Bonferroni correction. (B) The caudal region of MGv as a thalamic origin of A2. Data in blue, green, and red indicate distributions of neurons projecting to AAF, A1, and A2, respectively. Averaged coordinates were 3.03 mm, 3.13 mm, and 3.93 mm posterior to the bregma for AAF, A1, and A2, respectively. The A2 datasets were the same in (A) and (B), and the AAF and A1 data were obtained by injecting fluorescent CTB into 10-kHz areas. AAF vs. A1, $P < 10^{-35}$; AAF vs. A2, $P < 10^{-35}$; A1 vs. A2, $P < 10^{-35}$, $\chi^2$ test after Bonferroni correction. To AAF, $n = 1,314$ cells (five mice); to A1, $n = 510$ cells (five mice); To A2, $n = 2,718$ cells. (C) Confirmation of caudal outputs to A2 using horizontal slices. Neurons projecting to A2 (red) were located significantly more caudally than those projecting to A1 (green) (**$P < 0.0001$; ***$P < 10^{-34}$, Mann–Whitney $U$-test; $n = 196$ neurons projecting to A1; $n = 198$ neurons projecting to A2; from three mice). BIC, brachial nucleus of the inferior colliculus; CNLP, caudal non-lemniscal pole. Scale bar, 200 μm. Data are shown in mean ± SEM.

## Frequency-Related Organization in Higher-Order Auditory Thalamus, MGd

In addition to the newly discovered inputs from MGv, we also confirmed that A2 receives projections from MGd. Triple tracer injection revealed that MGd neurons between 3.0 and 3.4 mm posterior to the bregma projected to A2, and that, for tonal stimuli between 5 and 60 kHz, the rostrocaudal distributions of neurons that project to each part of A2 did not differ (Supplementary Fig. 4A). After injecting retrograde tracers into A2, the number of labeled neurons in MGd was small and few slices exhibited neurons that were labeled by all three tracers; however, we did observe positional shifts of labeled neurons (Supplementary Fig. 4B). We quantitatively analyzed the locations of labeled neurons by determining the center of MGd as the origin (Supplementary Fig. 4C) and found that positions shifted from dorsomedial to ventrolateral MGd as the BFs of the target region in A2 shifted from high to low. Although we cannot presently conclude that this structure is tonotopic, to the best of our knowledge this is the first study to demonstrate the existence of frequency-related organization in rodent MGd. Additionally, neurons found in the non-lemniscal caudal pole of the MGB which were retrogradely labeled exhibited topographical shifts in the ventrodorsal direction (Supplementary

Fig. 5). Because the direction of topographical shift differed between neurons labeled in MGd and those in the caudal non-lemniscal pole of the MGB, the caudal non-lemniscal pole of the MGB might be functionally separate from MGd.

## Tonotopy of A2 is Established via Thalamic Input

A2 is a higher-order region that receives auditory information from A1. However, our results showed that it also receives distinct topographical input from the thalamus. This suggested that tonotopic organization in A2 might exist even when it is isolated from primary cortical regions. To test this hypothesis, we prepared mice in which all auditory cortical regions except for A2 were removed by suction (Fig. 6A). A2 in these mice still exhibited robust tonal responses (Fig. 6B). While no tonal responses were detected from the removed regions, in A2 they remained even after suction, albeit they were half as intense (Fig. 6C,D), suggesting that responses in A2 were derived both corticocortically and thalamocortically. Importantly, the tonotopic structure of A2 remained after destroying the surrounding cortical regions (Fig. 6E,F). Moreover, we verified that functional organization in the auditory cortex and response amplitude elicited by amplitude-modulated pure tones was not affected by total
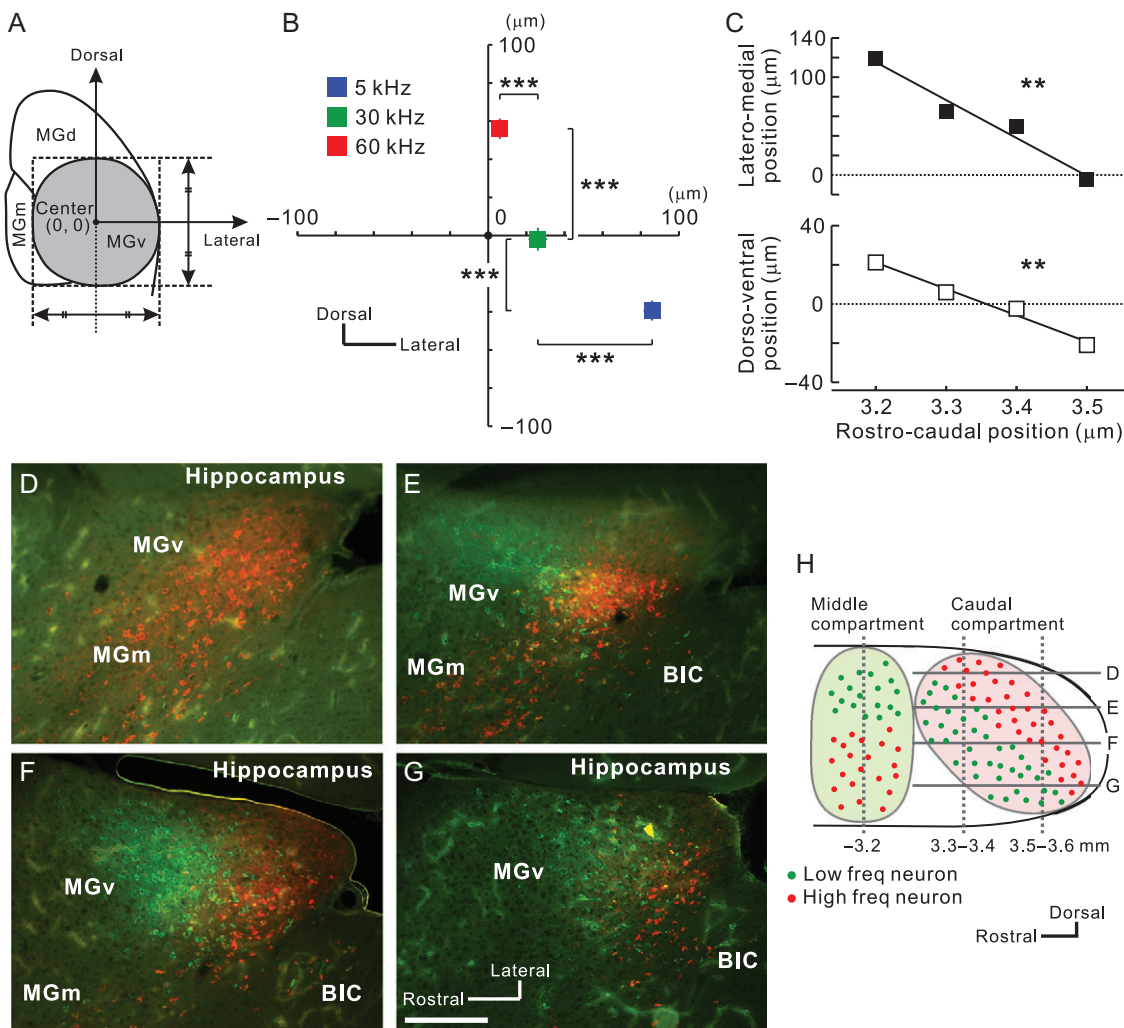
**Figure 5.** Frequency-related gradient traveling ventrodorsally in caudal MGv. (A) Definition of the MGv center in each slice. (B) Average coordinates for projection neurons to A2 in slices 3.2–3.6 mm posterior to the bregma. The number of neurons was 1 268 for 5 kHz, 593 for 30 kHz, and 825 for 60 kHz. ***P < 0.001, Mann–Whitney U-test. (C) Lateromedial (top) and dorsoventral (bottom) shift of average coordinates for projection neurons to A2 in slices along 3.2–3.5 mm posterior to the bregma. Zero indicates the center of MGv obtained as shown in (A). **P < 0.01, Spearman's test. (D–H). View of the caudal compartment of MGv. Horizontal distribution of MGv neurons projecting to low (green) and high (red) frequency areas in A2 are shown in (D–G). Scale bar, 200 μm. Approximate dorsoventral levels of each image are indicated in (H). Data are shown in mean ± SEM.

removal of the contralateral auditory cortex (Supplementary Fig. 6A–C). This might have resulted from callosal connections that help unify auditory space (Gazzaniga 2000) and are not necessary for simple tonal processing. To consolidate these findings, we confirmed that A2 was activated by tonal presentation and its tonotopy was retained after the whole contralateral auditory cortex and ipsilateral auditory cortical fields except A2 were removed in the same animal (Supplementary Fig. 6D–F). These data suggest that parallel topographical thalamocortical pathways from MGv give rise to the different tonotopies seen in A2 and A1 in cooperation with input from MGd (Fig. 9).

## Consistency Between Thalamocortical Structure and Auditory Cortical Tonotopy Across Regions

Previous tracer studies have shown that two neuronal populations that project to areas of low and high frequency in A1 exhibited little spatial overlap in middle MGv (Horie et al. 2013; Takemoto et al. 2014). In contrast, caudal MGv neurons that

project to A2 exhibited seemingly overlapping distributions, although they also showed a ventrodorsal tonotopic gradient at the macroscopic level (Fig. 2, Supplementary Fig. 7). To quantify and compare the degree of spatial overlap in the MGv neuronal populations, we dual-injected CTB-555 and CTB-488 into high and low frequency areas of A1 and A2, respectively (Fig. 7A). An analysis of spatial spread in four directions showed that neurons projecting to A2 were distributed more widely than those projecting to A1 in the dorsoventral direction, which corresponds to the tonotopic axis (Fig. 7B). As a result, the separation index along the dorsoventral axis was significantly smaller for neurons projecting to A2 than for those projecting to A1 (Fig. 7C). These data suggest that local areas of A1 receive thalamic input from a somewhat narrow area within the middle part of MGv. In contrast, local areas of A2 receive thalamic input from a broader area within the caudal part of MGv, which may be a result of projectional convergence/divergence and arborization of axonal collaterals.

Studies have suggested that BF spatial distribution becomes more heterogeneous the further a layer and region are along in
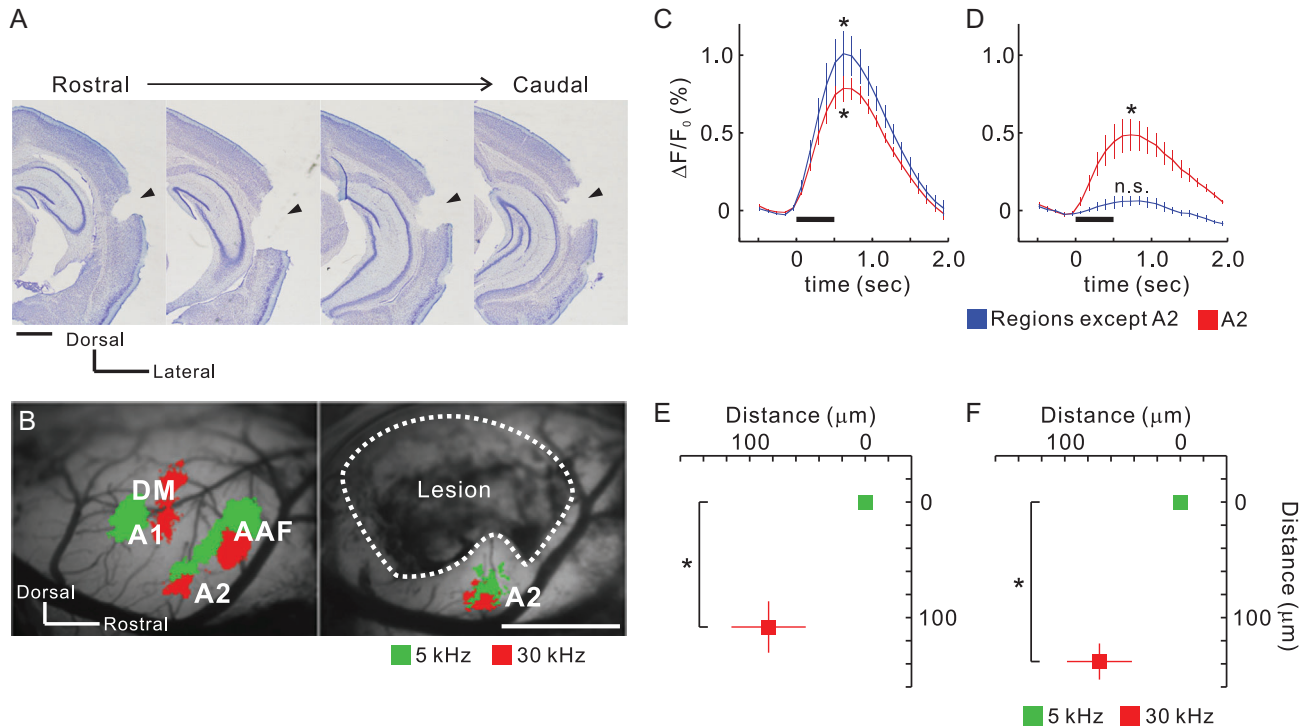
**Figure 6.** Retained tonotopy in A2 after removal of other auditory regions. (A) Coronal slices from the right hemisphere after suction of auditory cortex that excluded A2. Lesion sites are indicated by arrow heads. Scale bar, 1 mm. (B) Example tonal responses in A2 before and after suction in the same animal. Areas enclosed by dotted lines were removed and the white matter on the hippocampus was exposed. Scale bar, 1 mm. (C and D) Temporal profiles of tonal responses before (C) and after suction (D). Data from regions other than A2 are average values from AAF, A1, and DM. Peak values were significantly larger than baseline values. *$P < 0.05$, Wilcoxon signed-rank test. Four profiles were obtained from the same animals ($n = 5$ mice). (E and F) Quantitative analysis of tonotopic shifts before (E) and after suction (F). Coordinates were averaged based on the peak pixels of 5 kHz areas. *$P < 0.05$, Wilcoxon signed-rank test. Four data were obtained from the same animals ($n = 5$ mice). Data are shown in mean ± SEM.

the hierarchy away from the input layer of the primary cortex (Winkowski and Kanold 2013; Issa et al. 2014). Inter-regional differences between A1 and A2 in the heterogeneity of the BF spatial distribution and frequency tuning have been investigated in layer 2/3 (Issa et al. 2014); however, we expected that neurons in the thalamocortical recipient layer of A2 would exhibit broader tuning and more heterogeneous BF distribution than what we observed in A1 via two-photon calcium imaging because thalamocortical structures terminating in A1 and A2 were different. Thalamocortical recipient layers in the auditory cortex are a deeper part of layer 3 and layer 4 (Huang and Winer 2000). They are equivalent to layers 3b/4 in mice, which are located ~300–450 mm beneath the cortical surface (Oviedo et al. 2010; Winkowski and Kanold 2013; Zhou et al. 2014). We observed tonal responses of neuronal cell bodies 377 ± 41 μm (mean ± SD) beneath the cortical surface (Fig. 8A, Supplementary Fig. 8). Neurons in A1 tended to respond to a specific tonal stimulus. In contrast, neurons in A2 had a tendency to respond to a wider frequency range (Fig. 8B) in our specific experimental condition. Analysis showed that neuronal bandwidth was significantly larger in A2 than in A1 (Fig. 8C). Next, we investigated differences in BF spatial distribution between A1 and A2. Although a study has suggested that local BF spatial distribution in the recipient layer of A1 was totally homogeneous (Winkowski and Kanold 2013), here we found that it was somewhat heterogeneously arranged (Fig. 8D). Even so, the BF and distance along the tonotopic axis were significantly correlated in A1 ($r = 0.61$; Fig. 8E, Supplementary Fig. 8C), as were the difference in BFs and the distance between pairs of neurons ($r = 0.43$; Fig. 8F). In contrast, the spatial distribution of BFs was

coarse in A2. Although the BF and distance along the tonotopic axis were significantly correlated ($r = 0.30$; Fig. 8G,H, Supplementary Fig. 8C), the correlation was much weaker than what we observed for A1. Similarly, although we found a significant correlation between the difference in BFs and the distance between pairs of neurons, the correlation coefficient ($r = 0.15$) was clearly smaller than that for A1 (Fig. 8I), and the difference in BFs between pairs of neighbor neurons was larger in A2 than in A1 (Supplementary Fig. 8D). These results are consistent with our hypothesis that inputting wide ranges of thalamic information to local areas of A2 may be one of the mechanisms that provide broader tuning and more complex functional organization in the thalamocortical recipient layer of A2.

## Discussion

### Mouse A2 is a Higher-Order Auditory Field, but Receives Lemniscal Input

In the classical view, the auditory cortex is composed of the core and belt regions (Kaas and Hackett 2000). By definition, the core comprises the primary regions such as A1/AAF that are centrally localized and have tonotopy that reflects thalamic input from MGv. The belt comprises non-tonotopic, higher-order regions that receive non-lemniscal thalamic inputs from MGd. Mouse A2 has been considered as part of the belt because electrophysiological mapping indicated no clear tonotopic arrangement (Stiebler et al. 1997). However, more recent studies have shown that mouse A2 does indeed have distinct tonotopy
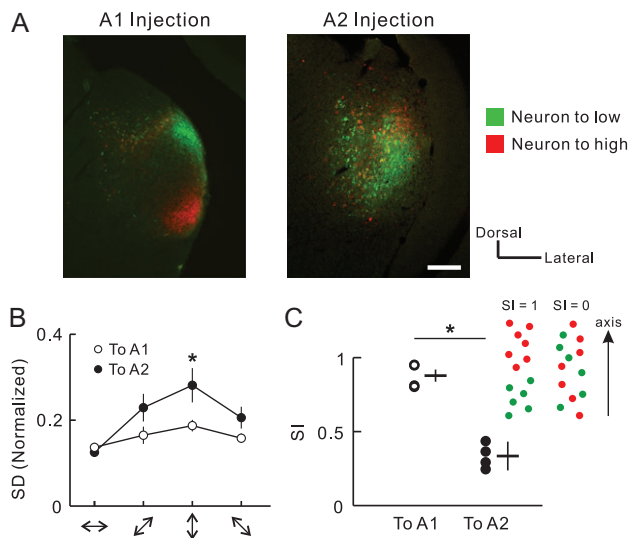
**Figure 7.** Widely-distributed MGv neurons which project to A2. (A) Examples of MGv neurons projecting to A1 or A2. Images depict coronal sections of the middle and caudal parts of MGv after injecting CTB-488 and CTB-555 into different frequency areas in two different animals. Scale bar, 200 μm. Green, CTB-488 that was injected into a cortical low frequency area of 5 kHz. Red, CTB-555 that was injected into a cortical high frequency area of 60 kHz. The right image was modified in brightness. Scale bar, 200 μm. (B) Standard deviations (SD) of the distribution of CTB-positive neurons in four orientations. SD was compensated by width and length of MGv. $n = 8$ slices from four mice. *$P < 0.05$, Mann–Whitney $U$-test. (C) The separation index (SI) that evaluates the extent to which CTB-488-positive and CTB-555-positive neurons are intermingled. SI ranges from 0 to 1, with one meaning total separation (see Methods). Data were obtained from four slices for each region. *$P < 0.05$, Mann–Whitney $U$-test.

(Kubota et al. 2008; Issa et al. 2014), and the current study shows that the tonotopy in A2 also reflects topographical thalamic input derived from MGv (Fig. 4). This suggests that mouse A2 which is physiologically identified may belong to the core rather than to the belt. To date, we know of four tonotopic regions in the auditory cortex—AAF, A1 A2, and DM (Tsukano et al. 2015)—and one tonotopic region in the insular cortex— the insular auditory field (IAF) (Takemoto et al. 2014). All of these regions receive substantial projections from MGv (Tsukano et al. 2017a). Such multiple tonotopic fields have been found in rats as well (Storace et al. 2010, 2012), and therefore might be ubiquitous in the rodent auditory system.

The presence of multiple tonotopic regions that receive lemniscal input does not mean that the hierarchy between auditory regions does not exist. Although a study in which sliced auditory cortex was stimulated suggested bidirectional processing between A1 and A2 (Covic and Sherman 2011), several *in vivo* studies suggest that compared with A1, mouse A2 has higher-order properties. For example, latencies for tonal presentation are longer in A2 than in A1 (Kubota et al. 2008; Guo et al. 2012). Additionally, the distribution of BFs for neighboring neurons in layer 2/3 (Issa et al. 2014) and, as shown here, layer 3b/4 (Fig. 8) is more mixed in A2 than in A1. Furthermore, A2 receives lemniscal thalamocortical input from a broader area than does A1 (Fig. 7). These findings imply that the nature of A2 is more complex than in the primary regions (Joachimsthaler et al. 2014). Moreover, other studies have shown that auditory information propagates unidirectionally even between canonical cores (AAF and A1) (Kubota et al. 2008; Zhang et al. 2017), suggesting that intracortical serial information processing along a hierarchical stream exists in the auditory cortex.

Overall, A2 should still be considered a higher-order region in the mouse auditory cortex, and thus the mouse auditory cortex serves as a good model for investigating serial information processing in the mammalian auditory system.

## Caudal MGv is a Thalamic Origin of Exogenous Inputs to A2

The auditory pathway is composed of two major and mutually exclusive canonical parallel streams: the lemniscal and non-lemniscal pathways. The lemniscal pathway conveys auditory information that retains the tonotopic structure that is generated in the ear, and enters AAF/A1 via MGv. The non-lemniscal pathway, whose origin is not clear, possibly conveys multimodal information to A2 via MGd. The current results show that caudal parts of MGv, as confirmed by calretinin immunolabeling, include a large amount of neurons that directly project to A2 (Fig. 4), which suggests that lemniscal information is fed into A2 from MGv. Past studies in mice (Llano and Sherman 2008) and cats (Lee and Winer 2008a) suggested that MGd was the origin of the thalamic inputs to A2. The present results confirm that A2 does receive non-lemniscal thalamic inputs from MGd, but clearly, the region does not have a single source of thalamic input.

The new scheme of thalamic inputs to A2 found in the present study is compatible with serial information transfer to A2 through the auditory cortical hierarchy. Generally, sensory information transfer to secondary fields is thought to be realized by corticocortical connections (Supplementary Fig. 9A). Direct projections from A1 to A2 have been found in mice (Covic and Sherman 2011) and cats (Lee and Winer 2008b), which are similar to those between primary and secondary fields in the visual (Glickfeld et al. 2013) and somatosensory (Chen et al. 2013) systems. The current study also strongly suggests that A2 receives corticocortical input from AAF/A1 because tonal responses in A2 were clearly reduced after removing all auditory cortical regions other than A2 (Fig. 6). Additionally, auditory information might be conveyed from A1 to A2 indirectly through corticothalamocortical loops, which compose A1–MGd–A2 projections (Supplementary Fig. 9B; Lee 2015). The latter possibility is supported by the presence of projections from A1 to MGd and from MGd to A2 in cats (Winer et al. 1999; Huang and Winer 2000;) and mice (Llano and Sherman 2008). Our results also confirmed the MGd to A2 pathway in mice (Supplementary Fig. 4). We also identified a third and previously unknown pathway that conveys tonal information directly from MGv to A2 without passing through A1 (Supplementary Fig. 9C). Actually, the presence of this pathway has been suggested in a cat study (Lee and Winer 2008a), although the idea has not caught on in the research community. Such parallel pathways from the primary thalamus to higher-order auditory fields have been found in rats (Storace et al. 2011; Shiramatsu et al. 2016), where cortical regional properties inherit properties of terminating thalamocortical axons (Storace et al. 2012). Integration of these three types of input in A2 is thought to be critical for realizing higher-order auditory function.

Some studies have reported that MGd is exclusively labeled after injecting retrograde tracers into mouse A2 (Ji et al. 2016). The discrepancy between these studies and our observation here could be related to two possibilities. First, the current study injected retrograde tracers iontophoretically with the guidance of optical imaging, which enables local injection by preventing tracers from spreading outside the precisely-identified target
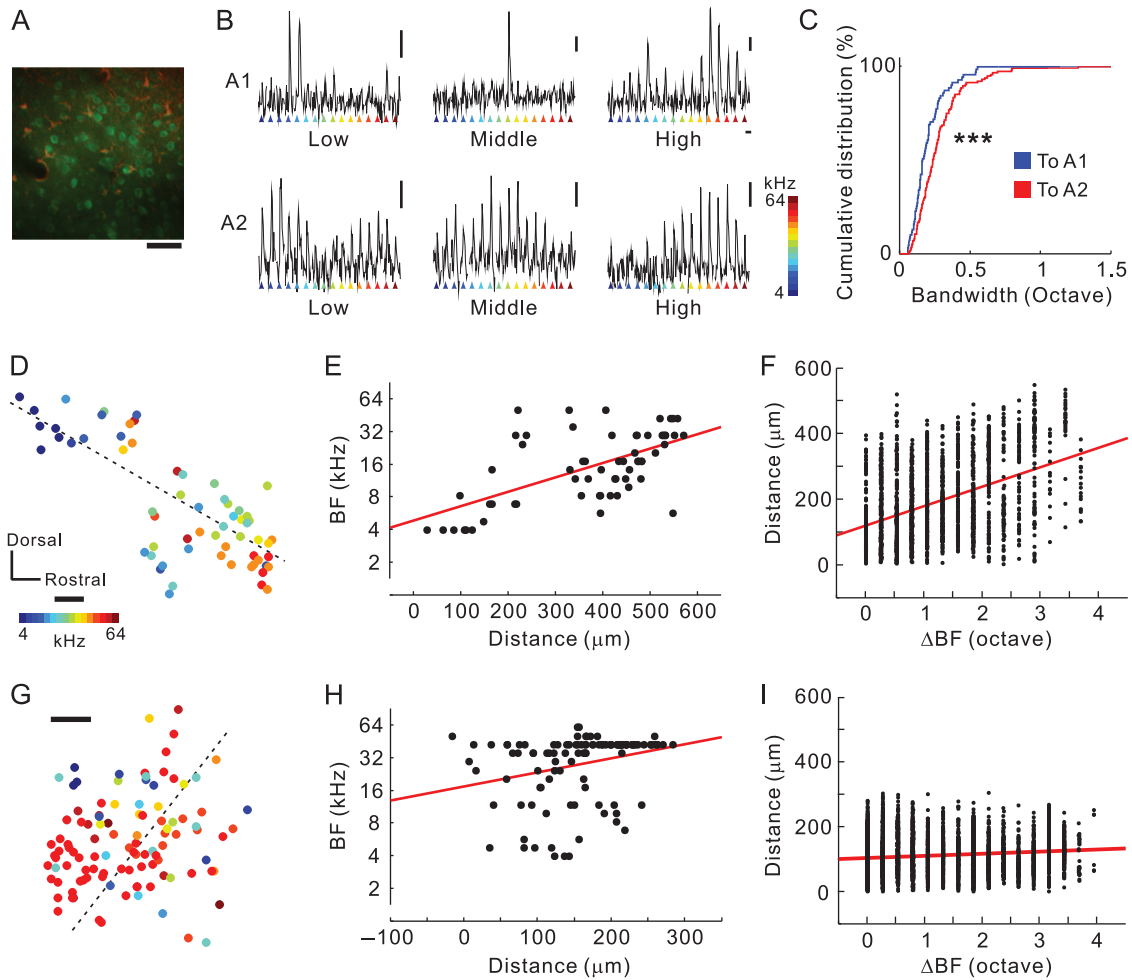
**Figure 8.** Complex responses of neurons in the thalamocortical recipient layer of A2. (A) An example plane of two-photon imaging. Cal-520-positive neurons and SR-101-positive astrocytes are shown in green and red, respectively. Scale bar, 50 μm. (B) Responses of a low, middle, and high frequency-responsive neuron in A1 (top), and those in A2 (bottom). Vertical bar, 10%; horizontal bar, 3 s. (C) Cumulative distribution of neuronal bandwidth in A1 and A2. ***$P < 10^{-10}$, Kolmogorov–Smirnov test. (D and E) Distribution of best frequencies (BF) in A1. A significant relationship was found between distance and best frequencies (BFs) ($n = 62$ neurons from four fields-of-view from two mice; $r = 0.61$, $P < 0.0001$, Spearman's test). The dotted line in (D) indicates the optimized tonotopic axis adopted in (E). Scale bar, 50 μm. (F) Relationship between differences in BF and distance (1 891 pairs, $r = 0.43$, $P < 0.0001$, Spearman's test). (G and H) Distribution of BFs in A2. A significant relationship was observed between distance and BF ($n = 108$ neurons from four fields-of-view from two mice; $r = 0.27$, $P < 0.01$, Spearman's test). The dotted line in (G) indicates the optimized tonotopic axis adopted in (H). R-values between data in (E) and (H) were significantly different ($P < 0.01$, see Methods). Scale bar, 50 μm. (I) Relationship between differences in BF and distance (5 778 pairs, $r = 0.13$, $P < 0.0001$, Spearman's test). R-values between data in (F) and (I) were significantly different ($P < 10^{-35}$, see Methods).

area. Because auditory regions in the mouse brain are small, blind procedures easily miss A2 and inject to neighboring cortical regions such as TeA/Ect that exclusively receive MGd projections (Supplementary Figs. 2 and 3). Moreover, if tracers are pressure-injected, they will likely spread to neighboring cortical regions. Second, the current study investigated the distribution of retrograde tracer-labeled neurons throughout the whole rostrocaudal MGB. Some studies have only examined rostral parts of MGB as an example after injecting retrograde tracers into A2. As the current study suggests that rostral parts of MGd project to A2 (Supplementary Fig. 4), while rostral MGv does not (Fig. 4), looking only at rostral MGB would lead to the conclusion that only MGd projected to A2 and MGv did not. In any case, the current study bridges the gap between A2 identified on the cortical surface using optical imaging and that identified in histological studies.

The compartmentalization of rodent MGv has been verified by recent studies as well as the current one. In cats, the lemniscal thalamocortical streams that connect MGv and auditory cortex are parallel because few MGv neurons project to both AAF and A1, even though the two neuronal groups projecting to AAF and A1 are not spatially segregated (Lee et al. 2004). Recent studies have suggested that mice have much clearer localization and compartmentalization of neuronal groups within MGv that are based on cortical target. Neurons projecting to DM, AAF, or A1 are localized in the rostral, medio-medial, or medio-lateral compartments of MGv, respectively, all of which have frequency-related topography (Horie et al. 2013; Tsukano et al. 2015; Tsukano et al. 2017a, 2017b). IAF in the insular cortex also receives topographical projections from the ventro-medial part of middle MGv (Takemoto et al. 2014). Finally, the current work revealed that A2 receives topographical projections from neurons in the caudal part of MGv. These facts suggest that the five topographical thalamocortical pathways convey some specific sound information whose cortical target is selected by gating in MGv (Blundon and Zakharenko 2013).
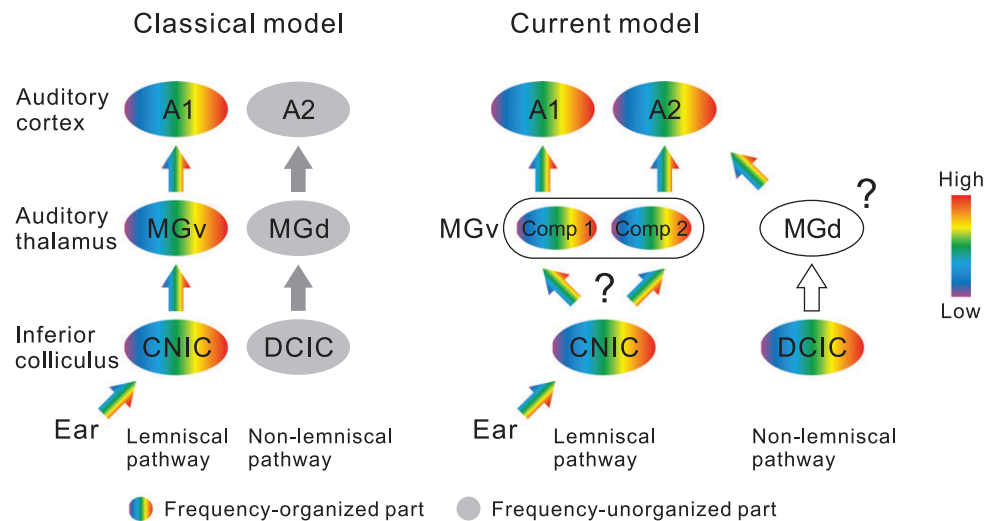
**Figure 9.** Illustration of a new thalamocortical parallel processing model in the mouse auditory system. The left illustration shows the classical two streams being fed into A1 and A2. These streams correspond to lemniscal and non-lemniscal pathways. The right illustration shows the new scheme based on the current results, in which the parallel lemniscal inputs feed into A1 and A2 in mice. Three points have not been clarified: (1) whether divergence of frequency organizations emerges when entering MGv from CNIC or not; (2) whether MGd reflects tonotopy; (3) and whether tectothalamic pathways between DCIC and MGd are connected topographically. CNIC, central nucleus of the inferior colliculus (IC); Comp, compartment; DCIC, dorsal cortex of IC.

Identifying the thalamic origins of A2 makes homologizing regions between animals easier. In mice, A2 sits the most ventrally in the auditory cortex (Fig. 1), its neurons have the longest response latency (Kubota et al. 2008; Guo et al. 2012), and MGv neurons projecting to A2 are localized caudally (Fig. 4). A similar fine-grained map and thalamocortical connections have been shown in rats (Polley et al. 2007; Storace et al. 2010). In rats, the suprarhinal auditory field (SRAF) is equivalent to mouse A2, being the most ventral tonotopic region with long response latency, and thalamic neurons projecting to SRAF are localized caudally in MGv (Storace et al. 2012). These common features between mouse A2 and rat SRAF indicate that they are homologous. Considering the presence of parallel thalamocortical inputs in cats, a common processing principle for mammalian audition might involve neuronal computations that integrate distinct thalamocortical and corticocortical inputs.

## Frequency Organization Differs Between A1 and A2

Previous two-photon imaging studies indicate that increased heterogeneity in BF distribution and broader tuning curves follow along the hierarchical streams in the auditory cortex (Winkowski and Kanold 2013; Issa et al. 2014). The current results indicate that the difference in frequency tuning and tonotopic heterogeneity between A1 and A2 exists in the thalamocortical recipient layer. These differences may be explained by thalamocortical neuroanatomy: The larger heterogeneity in BF distribution and broader tuning in A2 match the wide distribution of caudal MGv neurons that project to it (Fig. 7), and this anatomy could lead to the recently found heterogeneous BF distribution in presynaptic thalamocortical buttons (Vasquez-Lopez et al. 2017). Additionally, the relatively ordered tonotopy in the thalamocortical input layer of A1 is consistent with the somewhat localized neurons in the middle part of MGv that serve as its primary thalamic input. Finding this consistency between the thalamocortical anatomy and distinct functional properties in the cortex meshes nicely with an idea that tuning

curves in the auditory cortex are generally determined by thalamic inputs over intracortical circuits (Liu et al. 2007).

Other mechanisms for separating functional properties of different regions are also possible. Frequency tuning in L2/3 neurons has been reported to be modulated by intracortical network-level mechanisms in which inhibitory interneurons are involved (Kato et al. 2017); thus, frequency tuning in the thalamocortical recipient layer may also be modulated by local intracortical circuits. Moreover, A2 also receives thalamic input from MGd, which exhibits complex response patterns such as bursting in response to tones (He and Hu 2002) and broad bandwidth (Calford 1983) and which projects to the same layer that receives input from MGv (Llano and Sherman 2008). Although rise time of Cal-520 is shorter than that of GCaMP6f (Lock et al. 2015), Cal-520 signals are slow compared to electrophysiology; therefore, the current two-photon calcium imaging cannot fully distinguish between two thalamic inputs and intracortical activities. To solve this, further simultaneous recording of BFs from postsynaptic cortical somas and those from presynaptic buttons, which can be anterogradely-stained from the different compartments of MGv, would be necessary to fully characterize the differing contributions of thalamocortical projections. Anterograde tracing will be helpful because it visualizes branching patterns or arborization of axons to different frequency bands and different regions. According to Llano and Sherman 2008, projections from MGv to A2 may be sparser than those from MGd to A2. Moreover, it is also necessary to determine the functional organization and properties of MGv, as challenged by Hackett et al. (2011). At present, tonotopic organization and neuronal properties in multiple compartments of MGv are still unknown; frequency tuning might therefore already be broader in caudal parts of the MGv than the middle parts, and the auditory cortex might inherit this difference. Moreover, dendritic integration may make postsynaptic neuronal responses complex (Chen et al. 2011). Despite these limitations, the current study shows the presence of the direct MGv–A2 pathway and a glimpse of a thalamocortical anatomical mechanism that could change tuning and the local

functional organization, which might relate to the cortical hierarchy.

## Supplementary Material

Supplementary material is available at *Cerebral Cortex* online.

## Authors' Contributions

H.Ts. and K.S. first designed the study. S.O., H.Ts., and M.H. performed experiments. S.O., H.Ts., M.H., H.Te., and N.N. analyzed the data. Y.K. and K.T. provided critical ideas for planning this work. R.H. and H.Ta. provided critical comments regarding the results. S.O., H.Ts., and M.H. prepared the figures. H.Ts. wrote the manuscript. H.Ts. and K.S. revised the manuscript. All authors approved the publication of the manuscript.

## Funding

## Notes

## Declaration of Interests

The authors declare no conflict of interest.

## References

Allen Institute for Brain Science. 2011. Allen mouse brain atlas. Available at http://mouse.brain-map.org/.

Bandyopadhyay S, Shamma SA, Kanold PO. 2010. Dichotomy of functional organization in the mouse auditory cortex. Nat Neurosci. 13:361–368.

Bizley JK, King AJ. 2009. Visual influences on ferret auditory cortex. Hear Res. 258:55–63.

Blundon JA, Zakharenko SS. 2013. Presynaptic gating of postsynaptic synaptic plasticity: a plasticity filter in the adult auditory cortex. Neuroscientist. 19:465–478.

Cai D, Yue Y, Su X, Liu M, Wang Y, You L, Xie F, Deng F, Chen F, Luo M, et al. 2018. Distinct anatomical connectivity patterns differentiate subdivisions of the nonlemniscal auditory thalamus in mice. Cereb Cortex. *in press*. doi:10.1093/cercor/bhy115.

Calford MB. 1983. The parcellation of the medial geniculate body of the cat defined by the auditory response properties of single units. J Neurosci. 3:2350–2364.

Castro JB, Kandler K. 2010. Changing tune in auditory cortex. Nat Neurosci. 13:271–273.

Chen JL, Carta S, Soldado-Magraner J, Schneider BL, Helmchen F. 2013. Behaviour-dependent recruitment of long-range projection neurons in somatosensory cortex. Nature. 499: 336–340.

Chen X, Leischner U, Rochefort NL, Nelken I, Konnerth A. 2011. Functional mapping of single spines in cortical neurons in vivo. Nature. 475:501–505.

Cliff N. 1993. Dominance statistics: ordinal analyses to answer ordinal questions. Psychol Bull. 114:494–509.

Covic EN, Sherman SM. 2011. Synaptic properties of connections between the primary and secondary auditory cortices in mice. Cereb Cortex. 21:2425–2441.

de la Mothe LA, Blumell S, Kajikawa Y, Hackett TA. 2012. Thalamic connections of auditory cortex in marmoset monkeys: lateral belt and parabelt regions. Anat Rec. 295: 822–836.

Gazzaniga MS. 2000. Cerebral specialization and interhemispheric communication: does the corpus callosum enable the human condition? Brain. 123:1293–1326.

Glickfeld LL, Andermann ML, Bonin V, Reid RC. 2013. Cortico-cortical projections in mouse visual cortex are functionally target specific. Nat Neurosci. 16:219–226.

Guo W, Chambers AR, Darrow KN, Hancock KE, Shinn-Cunningham BG, Polley DB. 2012. Robustness of cortical topography across fields, laminae, anesthetic states, and neurophysiological signal types. J Neurosci. 32:9159–9172.

Hackett TA, Barkat TR, O'Brien BM, Hensch TK, Polley DB. 2011. Linking topography to tonotopy in the mouse auditory thalamocortical circuit. J Neurosci. 31:2983–2995.

Harel N, Mori N, Sawada S, Mount RJ, Harrison RV. 2000. Three distinct auditory areas of cortex (A1, A2, and AAF) defined by optical imaging of intrinsic signals. Neuroimage. 11: 302–312.

He J, Hu B. 2002. Differential distribution of burst and single-spike responses in auditory thalamus. J Neurophysiol. 88: 2152–2256.

Higgins NC, Storace DA, Escabí MA, Read HL. 2010. Specialization of binaural responses in ventral auditory cortices. J Neurosci. 30:14522–14532.

Honma Y, Tsukano H, Horie M, Ohshima S, Tohmi M, Kubota Y, Takahashi K, Hishida R, Takahashi S, Shibuki K. 2013. Auditory cortical areas activated by slow frequency-modulated sounds in mice. PLoS One. 8:e68113.

Horie M, Tsukano H, Hishida R, Takebayashi H, Shibuki K. 2013. Dual compartments of the ventral division of the medial geniculate body projecting to the core region of the auditory cortex in C57BL/6 mice. Neurosci Res. 76:207–212.

Horie M, Tsukano H, Takebayashi H, Shibuki K. 2015. Specific distribution of non-phosphorylated neurofilaments characterizing each subfield in the mouse auditory cortex. Neurosci Lett. 606:182–187.

Howell DC. 2012. Correlation and regression. In: Howell DC, editor. Statistical Methods for Psychology. 8th ed. Belmont (CA): Wadsworth. p. 251–301.

Huang CL, Winer JA. 2000. Auditory thalamocortical projections in the cat: laminar and areal patterns of input. J Comp Neurol. 427:302–331.

Imaizumi K, Lee CC. 2014. Frequency transformation in the auditory lemniscal thalamocortical system. Front Neural Circuits. 8:75.

Issa JB, Haeffele BD, Agarwal A, Bergles DE, Young ED, Yue DT. 2014. Multiscale optical Ca2+ imaging of tonal organization in mouse auditory cortex. Neuron. 83:944–959.

Ji XY, Zingg B, Mesik L, Xiao Z, Zhang LI, Tao HW. 2016. Thalamocortical innervation pattern in mouse auditory and visual cortex: laminar and cell-type specificity. Cereb Cortex. 26:2612–2625.

Joachimsthaler B, Uhlmann M, Miller F, Ehret G, Kurt S. 2014. Quantitative analysis of neuronal response properties in primary and higher-order auditory cortical fields of awake house mice (Mus musculus). Eur J Neurosci. 39:904–918.

Kaas JH, Hackett TA. 2000. Subdivisions of auditory cortex and processing streams in primates. Proc Natl Acad Sci USA. 97: 11793–11799.

Kalatsky VA, Polley DB, Merzenich MM, Schreiner CE, Stryker MP. 2005. Fine functional organization of auditory cortex revealed by Fourier optical imaging. Proc Natl Acad Sci USA. 102:13325–13330.

Kato HK, Asinof SK, Isaacson JS. 2017. Network-level control of frequency tuning in auditory cortex. Neuron. 95:412–423.

Kato HK, Gillet SN, Isaacson JS. 2015. Flexible sensory representations in auditory cortex driven by behavioral relevance. Neuron. 88:1027–1039.

Kubota Y, Kamatani D, Tsukano H, Ohshima S, Takahashi K, Hishida R, Kudoh M, Takahashi S, Shibuki K. 2008. Transcranial photo-inactivation of neural activities in the mouse auditory cortex. Neurosci Res. 60:422–430.

LeDoux JE, Ruggiero DA, Forest R, Stornetta R, Reis DJ. 1987. Topographic organization of convergent projections to the thalamus from the inferior colliculus and spinal cord in the rat. J Comp Neurol. 264:123–146.

LeDoux JE, Ruggiero DA, Reis DJ. 1985. Projections to the subcortical forebrain from anatomically defined regions of the medial geniculate body in the rat. J Comp Neurol. 242:182–213.

Lee CC. 2015. Exploring functions for the non-lemniscal auditory thalamus. Front Neural Circuits. 9:69.

Lee CC, Schreiner CE, Imaizumi K, Winer JA. 2004. Tonotopic and heterotopic projection systems in physiologically defined auditory cortex. Neuroscience. 128:871–887.

Lee CC, Sherman SM. 2008. Synaptic properties of thalamic and intracortical inputs to layer 4 of the first- and higher-order cortical areas in the auditory and somatosensory systems. J Neurophysiol. 100:317–326.

Lee CC, Sherman SM. 2010. Drivers and modulators in the central auditory pathways. Front Neurosci. 4:79–86.

Lee CC, Winer JA. 2008a. Connections of cat auditory cortex: I. Thalamocortical system. J Comp Neurol. 507:1879–1900.

Lee CC, Winer JA. 2008b. Connections of cat auditory cortex: III. Corticocortical system. J Comp Neurol. 507:1920–1943.

Li J, Zhang J, Wang M, Pan J, Chen X, Liao X. 2017. Functional imaging of neuronal activity of auditory cortex by using Cal-520 in anesthetized and awake mice. Biomed Opt Express. 8: 2599–2610.

Liu J, Whiteway MR, Butts DA, Kanold PO. 2017. Spatial organization of the mouse auditory cortex to sound dynamics revealed using automated image segmentation. bioRxiv. doi: http://dx.doi.org/10.1101/139659.

Liu BH, Wu GK, Arbuckle R, Tao HW, Zhang LI. 2007. Defining cortical frequency tuning with recurrent excitatory circuitry. Nat Neurosci. 10:1594–1600.

Llano DA, Sherman SM. 2008. Evidence for nonreciprocal organization of the mouse auditory thalamocortical-corticothalamic projection systems. J Comp Neurol. 507:1209–1227.

Lock JT, Parker I, Smith IF. 2015. A comparison of fluorescent $Ca^2+$ indicators for imaging local $Ca^2+$ signals in cultured cells. Cell Calcium. 58:638–648.

Lu E, Llano DA, Sherman SM. 2009. Different distributions of calbindin and calretinin immunostaining across the medial and dorsal divisions of the mouse medial geniculate body. Hear Res. 257:16–23.

Nishimura M, Shirasawa H, Kaizo H, Song WJ. 2007. New field with tonotopic organization in guinea pig auditory cortex. J Neurophysiol. 97:927–932.

Oviedo HV, Bureau I, Svoboda K, Zador AM. 2010. The functional asymmetry of auditory cortex is reflected in the organization of local cortical circuits. Nat Neurosci. 13: 1413–1420.

Paxinos G, Franklin KBJ. 2012. The Mouse Brain in Stereotaxic Coordinates. 4th ed.. San Diego (CA): Academic Press.

Petkov CI, Kayser C, Augath M, Logothetis NK. 2006. Functional imaging reveals numerous fields in the monkey auditory cortex. PLoS Biol. 4:e215.

Polley DB, Read HL, Storace DA, Merzenich MM. 2007. Multiparametric auditory receptive field organization across five cortical fields in the albino rat. J Neurophysiol. 97: 3621–3638.

Rothschild G, Nelken I, Mizrahi A. 2010. Functional organization and population dynamics in the mouse primary auditory cortex. Nat Neurosci. 13:353–360.

Saenz M, Langers DR. 2014. Tonotopic mapping of human auditory cortex. Hear Res. 307:42–52.

Shiramatsu TI, Takahashi K, Noda T, Kanzaki R, Nakahara H, Takahashi H. 2016. Microelectrode mapping of tonotopic, laminar and field- specific organization of thalamo-cortical pathway in rat. Neuroscience. 332:38–52.

Smith PH, Uhlrich DJ, Manning KA, Banks MI. 2012. Thalamocortical projections to rat auditory cortex from the ventral and dorsal divisions of the medial geniculate nucleus. J Comp Neurol. 520:34–51.

Stiebler I, Neulist R, Fichtel I, Ehret G. 1997. The auditory cortex of the house mouse: left-right differences, tonotopic organization and quantitative analysis of frequency representation. J Comp Physiol A. 181:559–571.

Storace DA, Higgins NC, Chikar JA, Oliver DL, Read HL. 2012. Gene expression identifies distinct ascending glutamatergic pathways to frequency-organized auditory cortex in the rat brain. J Neurosci. 32:15759–15768.

Storace DA, Higgins NC, Read HL. 2010. Thalamic label patterns suggest primary and ventral auditory fields are distinct core regions. J Comp Neurol. 518:1630–1646.

Storace DA, Higgins NC, Read HL. 2011. Thalamocortical pathway specialization for sound frequency resolution. J Comp Neurol. 519:177–193.

Tada M, Takeuchi A, Hashizume M, Kitamura K, Kano M. 2014. A highly sensitive fluorescent indicator dye for calcium imaging of neural activity in vitro and in vivo. Eur J Neurosci. 39:1720–1728.

Takemoto M, Hasegawa K, Nishimura M, Song WJ. 2014. The insular auditory field receives input from the lemniscal subdivision of the auditory thalamus in mice. J Comp Neurol. 522:1373–1389.

Tao C, Zhang G, Zhou C, Wang L, Yan S, Tao HW, Zhang LI, Zhou Y, Xiong Y. 2017. Diversity in excitation-inhibition mismatch underlies local functional heterogeneity in the rat auditory cortex. Cell Rep. 19:521–531.

Tsukano H, Horie M, Bo T, Uchimura A, Hishida R, Kudoh M, Takahashi K, Takebayashi H, Shibuki K. 2015. Delineation of a frequency-organized region isolated from the mouse primary auditory cortex. J Neurophysiol. 113:2900–2920.

Tsukano H, Horie M, Hishida R, Takahashi K, Takebayashi H, Shibuki K. 2016. Quantitative map of multiple auditory cortical regions with a stereotaxic fine-scale atlas of the mouse brain. Sci Rep. 6:22315.

Tsukano H, Horie M, Ohga S, Takahashi K, Kubota Y, Hishida R, Takebayashi H, Shibuki K. 2017a. Reconsidering tonotopic maps in the auditory cortex and lemniscal auditory thalamus in mice. Front Neural Circuits. 11:14.

Tsukano H, Horie M, Takahashi K, Hishida R, Takebayashi H, Shibuki K. 2017b. Independent tonotopy and thalamocortical projection patterns in two adjacent parts of the classical primary auditory cortex in mice. Neurosci Lett. 637: 26–30.

Vasquez-Lopez SA, Weissenberger Y, Lohse M, Keating P, King AJ, Dahmen JC. 2017. Thalamic input to auditory cortex is locally heterogeneous but globally tonotopic. eLife. 6:e25141.

Wang Q, Burkhalter A. 2007. Area map of mouse visual cortex. J Comp Neurol. 502:339–357.

Winer JA, Larue DT, Huang CL. 1999. Two systems of giant axon terminals in the cat medial geniculate body: convergence of cortical and GABAergic inputs. J Comp Neurol. 413:181–197.

Winkowski DE, Kanold PO. 2013. Laminar transformation of frequency organization in auditory cortex. J Neurosci. 33: 1498–1508.

Zhang G, Tao C, Zhou C, Yan S, Wang Z, Zhou Y, Xiong Y. 2017. Excitatory effects of the primary auditory cortex on the sound-evoked responses in the ipsilateral anterior auditory field in rat. Neuroscience. 361:157–166.

Zhou M, Liang F, Xiong XR, Li L, Li H, Xiao Z, Tao HW, Zhang LI. 2014. Scaling down of balanced excitation and inhibition by active behavioral states in auditory cortex. Nat Neurosci. 17: 841–850.